nature chemistry

Article

https://doi.org/10.1038/s41557-022-01107-8

Quantum interference effects elucidate triplet-pair formation dynamics in intramolecular singlet-fission molecules

Received: 16 March 2022

Accepted: 3 November 2022

Published online: 30 December 2022

Check for updates

Kaia R. Parenti[1], Rafi Chesler[2], Guiying He[3,4], Pritam Bhattacharyya[5], Beibei Xiao[6], Huaxi Huang[1], Daniel Malinowski[1], Jocelyn Zhang[1], Xiaodong Yin[6], Alok Shukla[7], Sumit Mazumdar[2,8] ✉, Matthew Y. Sfeir[3,4] ✉ & Luis M. Campos[1] ✉

Quantum interference (QI)—the constructive or destructive interference of conduction pathways through molecular orbitals—plays a fundamental role in enhancing or suppressing charge and spin transport in organic molecular electronics. Graphical models were developed to predict constructive versus destructive interference in polyaromatic hydrocarbons and have successfully estimated the large conductivity differences observed in single-molecule transport measurements. A major challenge lies in extending these models to excitonic (photoexcited) processes, which typically involve distinct orbitals with different symmetries. Here we investigate how QI models can be applied as bridging moieties in intramolecular singlet-fission compounds to predict relative rates of triplet pair formation. In a series of bridged intramolecular singlet-fission dimers, we found that destructive QI always leads to a slower triplet pair formation across different bridge lengths and geometries. A combined experimental and theoretical approach reveals the critical considerations of bridge topology and frontier molecular orbital energies in applying QI conductance principles to predict rates of multiexciton generation.

Quantum interference (QI) effects have been invoked as an important mechanism to control charge and/or spin transport properties in molecular electronics[1,2]. For conduction pathways connected by alternant hydrocarbons, subtle variations in bond connectivity can impact conditions that lead to constructive or destructive quantum interference (CQI and DQI, respectively)[3,4]. The classic example involves comparing transport between 1,3-phenylene (**13Ph**) and 1,4-phenylene (**14Ph**) bridges, in which the conductance of the **13Ph** bridge is decreased by several orders of magnitude due to DQI[5,6]. Graphical models were established to predict molecular bridges that yield DQI and CQI as they pertain to phase-coherent charge transport through frontier molecular orbitals (FMOs) in conjugated systems[7,8]. This method involves drawing a continuous path from one connection point to the other and pairing up atoms in the alternate path. If there is

[1]Department of Chemistry, Columbia University, New York, NY, USA. [2]Department of Physics, University of Arizona, Tucson, AZ, USA. [3]Department of Physics, Graduate Center, City University of New York, New York, NY, USA. [4]Photonics Initiative, Advanced Science Research Center, City University of New York, New York, NY, USA. [5]Institute for Theoretical Solid State Physics, Leibniz IFW Dresden, Dresden, Germany. [6]Key Laboratory of Cluster Science, Ministry of Education of China, Beijing Key Laboratory of Photoelectronic/Electrophotonic Conversion Materials, School of Chemistry and Chemical Engineering, Beijing Institute of Technology, Beijing, P. R. China. [7]Department of Physics, Indian Institute of Technology Bombay, Mumbai, India. [8]Department of Chemistry and Biochemistry, University of Arizona, Tucson, AZ, USA. ✉e-mail: mazumdar@email.arizona.edu; msfeir@gc.cuny.edu; lcampos@columbia.edu

https://doi.org/10.1038/s41557-022-01107-8

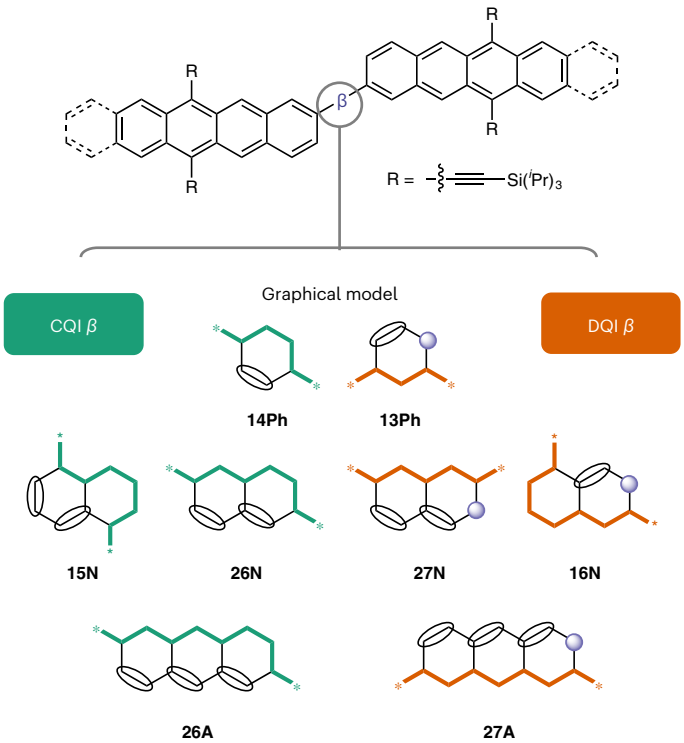

Fig. 1 | Model systems designed to investigate the role of QI. The bridged dimers PβP and TβT (top), where β = **14Ph**, **13Ph**, **15N**, **26N**, **27N**, **16N**, **26A** and **27A**. The DQI bridging patterns (orange), which include **13Ph**, **16N**, **27N** and **27A**, are expected to decrease the rate of SF relative to that of the CQI ones (green), **14Ph**, **15N**, **26N** and **26A**.

an odd number of atoms in the alternate path such that not all atoms are part of a pair, DQI is expected (Fig. 1). A similar set of principles were applied to biradical systems (Ovchinnikov's rule and related theorems) and used to predict the relative stabilities of the open-shell singlet and triplet states[7,9].

The applicability of graphical QI models as a predictive tool for photoexcited (excitonic) processes in donor–bridge–acceptor (DBA) chromophores is less established. A key difference is that photoexcited charge transfer (CT) involves excited-state orbitals on donor and acceptor sites that may exhibit different symmetries from each other and from those involved in conductance measurements[10]. As such, conditions for constructive interference are more difficult to generalize and require support from high-level quantum chemical calculations. For example, Grozema and co-workers studied photoinduced electron and hole transfer in DBA chromophores and found that QI could not be readily predicted from the connectivity of the bridge alone[11]. To explain differences in CT rates for different bridge connectivities, it was necessary to also account for symmetry relations of the donor, bridge and acceptor. These important fundamental results highlight the additional complexity inherent in describing dynamical photoexcited processes, which includes identifying key molecular orbitals and quantifying their character, relative energy, symmetries and coupling strength. Computational modelling is thus essential to characterize the QI effects in DBAs and other excited-state systems.

More recently, bridged singlet-fission chromophores (SFCs) have emerged as promising light-harvesting candidates for optoelectronic and chemical applications[12–17]. These intramolecular singlet-fission (iSF) compounds exhibit long-lived multiexciton states (in the form of a coupled triplet pair) that extend over multiple chromophores. Studies by various groups revealed the critical role of the bridging unit (β) in modulating the coupling between two (or more) SFCs and dictating the rate of triplet pair formation and decay and have additionally noted non-trivial effects related to connectivity[15,18–22]. However, the impact of QI effects and bridge connectivity on the singlet-fission (SF) dynamics in these systems remains largely unexplored. The exceptions are a discussion of spatially dependent coupling strengths in molecular crystals[23] and a recent suggestion that bridge connectivity can modulate triplet pair binding energies[24], although this is only one consideration[24,25]. To date, there is no comprehensive model to apply QI concepts to multiexcitonic organic systems. Importantly, the platform of iSF systems offers versatility to study the role of QI because covalent linkages and chromophores can be varied to access different conjugation and orbital symmetry patterns[26]. Furthermore, clear spectroscopic observables exist that allow for precise correlations to be made regarding the nature of the QI and its influence on the rate of triplet pair formation. Defining the role of QI in SF would provide an important understanding of how bridge structure can be used to optimize electronic communication between SFCs and, more broadly, how conductance principles can be extended to multiexcitonic systems.

Here we report how competing and coexisting QI effects drastically impact the rates of triplet pair formation in bridged homodimers (SFC–β–SFC). We posit that graphical models of QI can be used to understand the topological effects of bridging units in symmetric chromophores. To test the generality of this hypothesis, we used three alternant hydrocarbon bridges (phenylene (Ph), naphthalene (N) and anthracene (A)) for which graphical models of the QI patterns are well characterized[8,27]. Fig. 1 shows the predicted CQI (**14Ph**, **26N**, **15N** and **26A**) and DQI (**13Ph**, **16N**, **27N** and **27A**) structures for each bridge that links two pentacene (P) or tetracene (T) chromophores (P–β–P and T–β–T, respectively). We found that QI effects can be predicted by graphical models in all the compounds, with triplet pair formation being slower for any β that exhibits DQI. However, as we move from the smaller Ph bridge to the larger N and A bridges, we found that it is also important to consider other factors (which include molecular geometry and resonance between the SFC and bridge FMOs) to obtain a holistic picture of the SF rate constant. Importantly, we identified a distinct correlation between the strength of the CT absorption resonances in the linear absorption spectra and the relative rates of iSF. These studies reveal the critical nature of chromophore connectivity in controlling the formation of the triplet pair and the necessity of combined experimental and theoretical approaches to understand chemical design principles. From these observations, we speculate that implementing QI principles in the design of SFCs using established guidelines[7] can lead to new systems with potential applications in quantum information and spin filters[28].

Results and discussion

Triplet pair formation rates in bridged molecules

We observed SF in all the SFC–β–SFC compounds and found that the rate constants for triplet pair formation were markedly different for DQI connectivity, consistent with the graphical model (Fig. 1). Importantly, the QI-type effects persisted across all the bridges used in this study. For both pentacene and tetracene compounds (P–β–P and T–β–T), a faster triplet formation was observed when β = **14Ph**, **26N** and **26A**, compared with the corresponding DQI connectivity (β = **13Ph**, **27N** and **27A**). This effect is readily observed in the raw transient absorption data (Fig. 2a and Supplementary Figs. 1 and 2) and single wavelength kinetics selective for the rise of the triplet (pentacene, Fig. 2b) or decay of the singlet (tetracene, Fig. 2c). Comparing P–Ph–P compounds, τ_{SF} drastically changed by a factor of 23, from 17 ps for **P–14Ph–P** to a much slower 391 ps for **P–13Ph–P**. This effect was even more pronounced in the analogous T–Ph–T compounds, with a faster τ_{SF} of 7 ps for **T–14Ph–T** and a 65 times slower, 453 ps, in **T–13Ph–T**. Importantly, the DQI had a larger impact on the SF dynamics than the proximity of the bridged P and T SFCs. For example, the rate of SF in **13Ph** was about twice as slow as that of the previously reported 4,4′–biphenylene (β = **44bPh**) bridged

https://doi.org/10.1038/s41557-022-01107-8

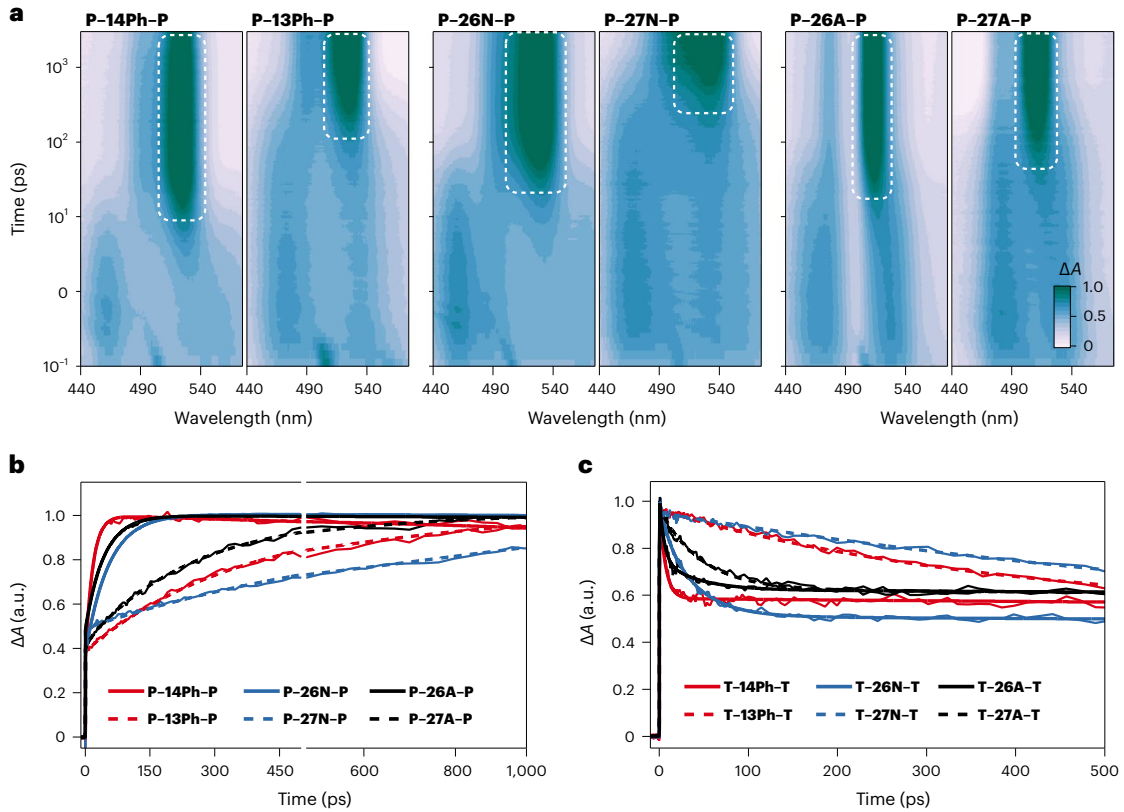

Fig. 2 | Determination of the time constants for triplet pair formation. a, Femtosecond transient absorption of pentacene compounds in dilute toluene solution (~50 μM) excited at 600 nm. Triplet photoinduced absorption (PIA) is in green and outlined for clarity. **b**,**c**, The single wavelength kinetics correspond to the rise of the pentacene triplet at ~520 nm (**b**) and decay of the tetracene singlet at ~455 nm (**c**) as a function of time. These data show that the rate of SF is always higher in the CQI versions of the molecules compared with that of the analogous DQI compounds. a.u., arbitrary units.

compounds **P–44bPh–P** (τ_{SF} = 220 ps) and **T–44bPh–T** (τ_{SF} = 240 ps), which have double the bridge length[29,30]. This result underlines the importance of bridge connectivity[18,31,32] in dictating triplet pair formation dynamics.

Interestingly, we found that the magnitude of the difference between the DQI and CQI effects diminished with increasing bridge length in the order **Ph** > **N** > **A**. Analogous to Ph-bridged compounds, large differences in the rate constants between the DQI (**27N**) and CQI (**26N**) connectivity points were observed in the N-bridged dimers. Triplet pair formation was slower in the **27N** DQI bridge relative to that in the **26N** CQI bridge by a factor of 16 in the pentacene series and by a factor of 32 in the tetracene series. These differ in magnitude compared with the 23-fold and 65-fold differences, respectively, for the Ph-bridged compounds. Furthermore, triplet pair formation in the **27A** DQI bridge relative to that in the **26A** CQI bridge was a factor of five slower for PβP and a factor of four slower for TβT, a more subtle difference than that observed for Ph and N bridges. A summary of iSF time constants for these compounds is shown in Table 1. The trends are depicted graphically in Fig. 3, where the plots are the normalized SF rate as a function of chromophore, bridge type and connectivity; and these are relative to the compound with the fastest rate of iSF in the series (**T–14Ph–T**). The monotonic decrease in the ratio of the rate of SF in CQI and DQI connectivities (k_{CQI}/k_{DQI}) is shown in Fig. 3, where it is clear that tetracene chromophores exhibit a larger contrast in rate constants with the smallest bridge, but this difference decreases with the longer bridges.

The decrease in the contrast of the SF rate constants between CQI and DQI connectivity (k_{CQI}/k_{DQI}) is not correlated to an overall decrease in the absolute magnitude of k_{SF}. The A bridge is notable in that, unlike the other bridges, the DQI compounds exhibit relatively fast rates of SF, although QI effects render them slower than those of the corresponding CQI compound. We previously reported how the FMOs of the bridges impact the rates of SF, as observed in **T–26A–T** (τ_{SF} = 14 ps), **P–26A–P** (τ_{SF} = 48 ps) and others[30]. As the FMOs of the bridging units approach resonance with those of the SF chromophores, the rates of triplet pair formation were enhanced. Here we found that this concept can also be extended to DQI bridge connectivity, such that moving from **P–13Ph–P** → **P–27N–P** → **P–27A–P** yielded an initial increase in τ_{SF} from 391 ps (**13Ph**) to 882 ps (**27N**) followed by a decrease to 253 ps (**27A**). With these considerations in mind, it can be reasoned that the bridge

Table 1 | Rate and time constants for SF in TβT and PβP

β	TβT		PβP	
	k_{SF} (ps^{-1})	τ_{SF} (ps)	k_{SF} (ps^{-1})	τ_{SF} (ps)
14Ph	1.43×10^{-1}	7	5.95×10^{-2}	17
13Ph	2.21×10^{-3}	453	2.56×10^{-3}	391
26N	3.33×10^{-2}	30	1.80×10^{-2}	56
27N	1.05×10^{-3}	952	1.13×10^{-3}	882
15N	1.69×10^{-3}	591	9.50×10^{-4}	1,053
16N	6.96×10^{-4}	1,437	5.51×10^{-4}	1,815
26A	7.14×10^{-2}	14	2.07×10^{-2}	48
27A	1.82×10^{-2}	55	3.96×10^{-3}	253

Uncertainties are ±5%. For more details on all the rate constants, see Extended Data Fig. 4.

https://doi.org/10.1038/s41557-022-01107-8

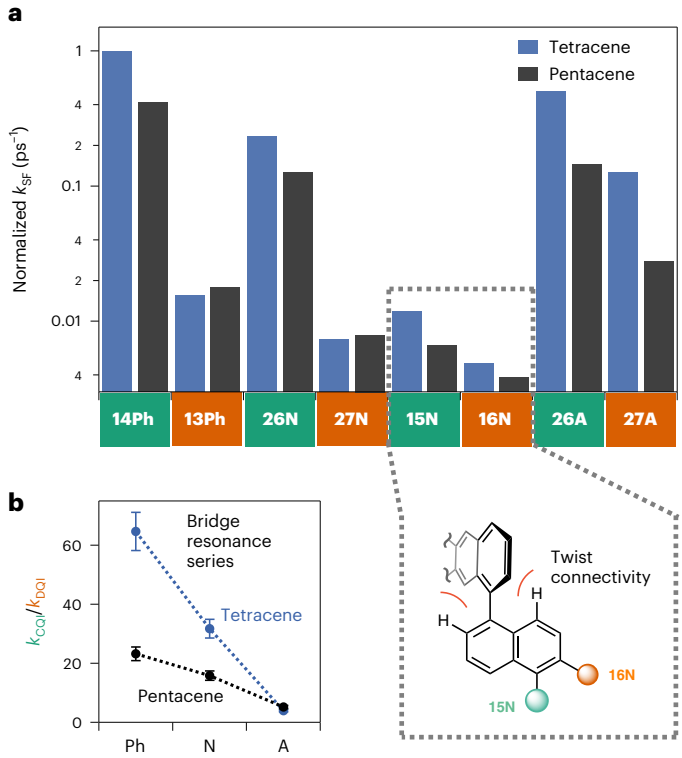

Fig. 3 | Comparison of SF rates (normalized to the largest k_{SF}) across all Ph, N and A bridges in this work. a, DQI (CQI) universally results in slower (faster) SF as denoted in the orange (green) boxes. Inset: Chromophores attached to the 1 and/or 5 positions of naphthalene exhibit larger dihedral angles than those attached to the 2, 6 or 7 positions, which reduces the overall planarity and slows SF, but still exhibit signatures of QI. **b**, For larger bridges, differences in the rate constants for CQI and DQI molecules become smaller due to contributions from the bridge frontier orbitals.

resonance effects have a stronger impact on the A-bridged DQI chromophores[30,33]. For example, the DQI chromophore **P–27A–P** underwent a faster iSF than that of **P–13Ph–P**, despite having a bridge that is longer by ~4.5 Å. Such a bridge resonance effect was even more pronounced in DQI tetracene analogues, for which τ_{SF} is reduced by a factor of 17 from 952 ps (**27N**) to 55 ps (**27A**). Although CQI compounds still underwent a faster iSF (48 ps for **P–26A–P** and 14 ps for **T–26A–T**) than those of their DQI counterparts (253 ps in **P–27A–P** and 55 ps in **T–27A–T**), the difference between the two connectivities was much less drastic than those within the Ph and N systems (Fig. 3).

Similar to how connectivity modulates bridge resonance effects, we found that QI considerations must also be accounted for in the limit of large geometric distortions, which have been shown to greatly reduce chromophore–chromophore coupling[34,35]. For example, in P–N–P, density functional theory calculations indicated (Extended Data Figs. 1 and 2) that chromophore attachments at the 1 and 5 positions were more twisted out of plane (~58°) than those at the 2, 6 or 7 positions (~35°). This allowed us to examine CQI and DQI in the highly twisted SFC couplings. We found that the β = **15N** CQI compounds underwent faster SFs (1.05 ns in **P–15N–P** and 591 ps in **T–15N–T**) than those of the DQI analogues (1.8 ns in **P–16N–P** and 1.4 ns in **T–16N–T**; Supplementary Fig. 2). We note that due to the QI effect, SF was actually faster in **15N**, in which both chromophores are more twisted than those in **16N**, in which only one chromophore is highly twisted. These trends agree with simple graphical models, even though the overall SF rates were relatively low due to the overall weak chromophore–chromophore coupling. The effect of weak electronic coupling in the highly distorted **15N** connectivity has also been observed in single-molecule junction experiments[36]. These results imply that QI remains a substantial effect in the limit of both strong and weak interchromophore coupling. Finally, given that the graphical model does not predict QI patterns in DBA chromophores due to the stark asymmetry of the systems, we further challenged how the model holds with slightly asymmetric T–β–P chromophores (β = **14Ph**, **13Ph**, **26N** and **27N**; Supplementary Figs. 11–13). These DBA-like chromophores had an inherent S_1/T_1 discrete energy offset between T and P (Supplementary Fig. 10). We found that **13Ph** and **27N** still exhibited a higher DQI (τ_{SF} = 355 ps and τ_{SF} = 863 ps, respectively) as compared with those of **14Ph** (τ_{SF} = 18 ps) and **26N** (τ_{SF} = 67 ps). With this in mind, we posit that other bridging units and architectural variations will spotlight QI effects in the design of iSF chromophores with tunable excited-state dynamics.

Excited-state wavefunction calculations

Although the above experimental observations highlight clear trends in the SF dynamics, they were not able to unambiguously identify the root causes of differences in the rate of triplet pair formation in DQI versus CQI compounds. For example, the triplet absorption spectra are not sharp enough to identify small differences in the electronic structures of the triplet pair for the two cases. Furthermore, these data are unable to assign the origin of the strong dependence of τ_{SF} on the length of the bridge molecule, that is, even DQI compounds with an A bridge have an unexpectedly fast SF. To capture these effects, we performed correlated-electron calculations of the excitonic states based on the π-electron-only Pariser–Parr–Pople (PPP) model[37,38]. A key feature of these calculations is that they include high-order configuration interactions, which include quadruple excitations over a large active space (Methods, Extended Data Fig. 3 and Supplementary Information). Using this approach, we determined the wavefunctions and energies of (1) bright singlet states that are dominated by Frenkel exciton configurations localized on the SFC (denoted as LE_T, LE_P and LE_A for tetracene, pentacene and anthracene, respectively) and bridge moieties (LE_β), (2) eigenstates with contributions from CT configurations between the SFC and bridge ($CT_{C\beta}$) as well as between the two SFCs (CT_{CC}) and (3) the lowest triplet pair eigenstate $^1(TT)$.

The effects of QI on the SF rate constants are expected to vary as a function of bridge length and electronic structure. Furthermore, QI should preferentially affect the CT-mediated SF processes[39,40]. A direct exchange mechanism has been shown to be important for SF when chromophores are directly coupled (no bridge) and when the singlet and triplet pair energies are nearly resonant[34]. In these systems, the rate constant is proportional to the matrix element: $k_{SF} \approx \left|\langle S_1|\, H_{el}^{(2)}\, |TT\rangle\right|^2$, where $H_{el}^{(2)}$ is the two-electron interaction term in the electronic Hamiltonian[39]. The relative importance of this pathway will diminish with increased chromophore separation and minimal QI effects are expected. In contrast, CT is a quantum mechanical process that can only occur between sites of opposite spins. For CT-mediated SF, matrix elements that involve the virtual CT state and its energetic offset affect the overall SF rate constant[39], $k_{SF} \approx \left|\langle S_1|\, H_{el}^{(1)}\, |CT\rangle \langle CT|\, H_{el}^{(1)}\, |TT\rangle / \Delta E_{CT}\right|^2$, where $H_{el}^{(1)}$ is the one-electron term in the electronic Hamiltonian and $|\Delta E_{CT}|$ is the energy difference between the CT state and the nearly degenerate S_1 and TT states[39]. Note that in iSF compounds, the CT between the SFC chromophores proceeds via a real or virtual CT between chromophore and bridge, which is the origin of bridge resonance. In the context of the compounds discussed here, graphical QI models predict that changing the bridge connectivity has the effect of flipping the spins on the SFC atoms connected to the bridge. In DQI, the probability that the two connecting atoms have the same spin is large, which reduces the effective CT character.

Here we present a comprehensive theoretical treatment of quantum effects in bridged iSF compounds that includes the effect of SFC connectivity, bridge length and the role of the FMOs of the bridge. Our calculations show that the widely different τ_{SF} values between DQI and

https://doi.org/10.1038/s41557-022-01107-8

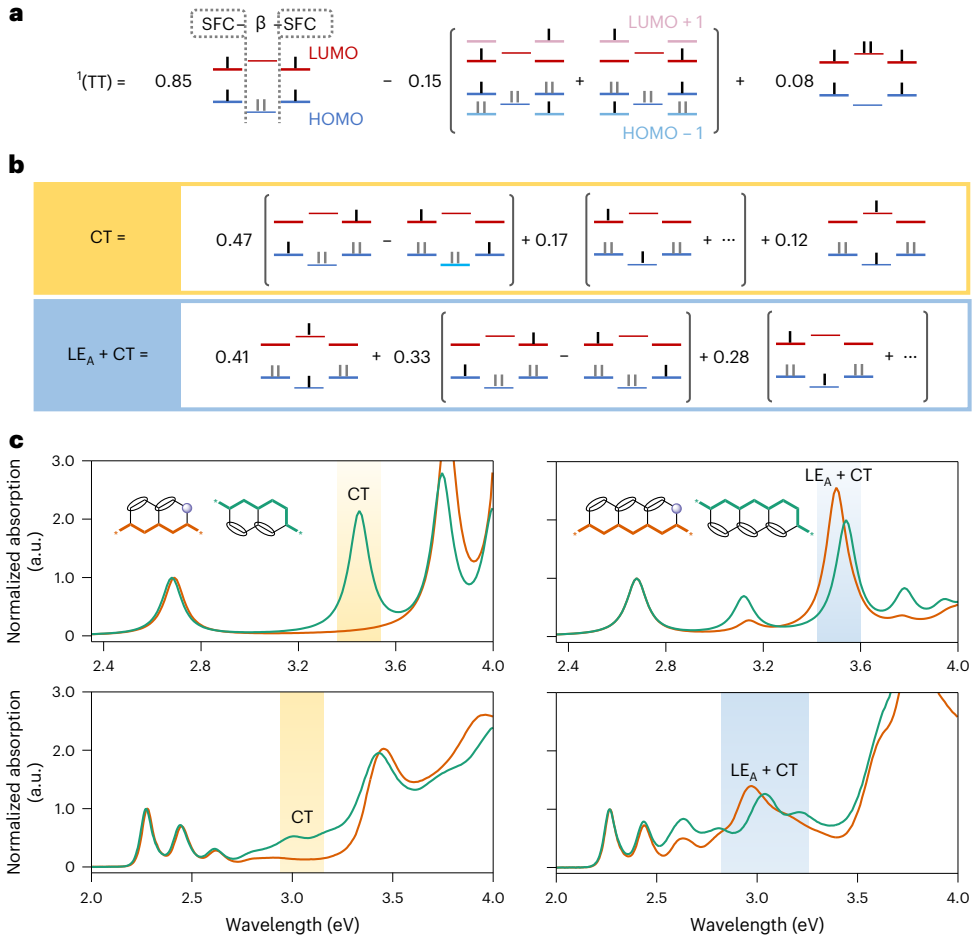

Fig. 4 | Contributions to the absorption spectra from the CT wavefunctions that mediate fast SF. a, Normalized triplet pair wavefunction for **T–26N–T** and **T–27N–T** in the molecular exciton-basis representation. The overall spin is zero for each individual configuration. Bonding molecular orbitals (MOs) not shown in any configuration are completely filled. Antibonding MOs not shown in any configuration are completely empty. **b**, Normalized CT wavefunctions for **T–26N–T** (yellow) and **T–26A–T** (blue). The latter exhibits substantial admixing with local excitation on the A monomer and is labelled accordingly. Ellipses correspond to additional terms related by mirror-plane and charge-conjugation symmetries. **c**, Calculated (top) and experimental (bottom) normalized absorption spectra for **T–N–T** (left) and **T–A–T** (right). Green traces correspond to a CQI bridge (**26N** or **26A**), orange traces correspond to a DQI bridge (**27N** or **27A**). Contributions to the absorption spectra from the CT wavefunctions depicted in **b** are highlighted and labelled. The calculations assume a planar conformation. The inclusion of intermonomer rotation decreases the intensity of the CT absorption, but the absorption energy is largely unaffected[41]. HOMO, highest occupied molecular orbital; LUMO, lowest unoccupied molecular orbital.

CQI compounds are not due to differences in their ^{1}(TT) wavefunctions. Instead, the calculated ^{1}(TT) eigenstates for all the compounds were overwhelmingly dominated by triplet excitations that occupy each of the terminal SFCs. Somewhat surprisingly, in the DQI and CQI SF compounds (except **14Ph** and **13Ph**), the ^{1}(TT) wavefunctions were nearly identical, independent of the nature of the bridge. The three most dominant contributions to the ^{1}(TT) eigenstate common to **T–26N–T** and **T–27N–T** are shown in Fig. 4a, with smaller contributions listed in Supplementary Fig. 7. To explicitly calculate these wavefunctions is important, as the ~30% additional contributions to the wavefunctions beyond the dominant two electron–two hole excitation contribute to the binding energy of ^{1}(TT)[41,42]. Although previous theoretical treatment suggested that the triplet pair states are fundamentally different for DQI versus CQI connectivity[25], our calculations show that this result does not extend to bridges longer than β = **Ph**.

Connecting charge-transfer character to graphical models

Instead, we show that ground-state absorption to an odd-parity CT state varies greatly with bridge connectivity and provides a direct measure of the interchromophore coupling necessary for an efficient SF. This conclusion follows from the graphical model that predicts the QI conditions: our PPP Hamiltonian conserves spin-symmetry requirements and optically allowed CT processes can only occur between sites that are antiferromagnetically coupled. There is thus a one-to-one correspondence between the strength of the transition-dipole coupling to the CT state and interchromophore coupling. In **T–26N–T** (Fig. 4b,c), for example, the most dominant term in the wavefunction that is the final state of the optical transition at ~3.5 eV is from a CT_{CC} configuration that involves a direct CT between the terminal tetracene molecules (Fig. 4b). Although a similar CT state also occurs in the DQI (**27N**) version of this compound, the transition dipole moment between the ground state and this CT state is nearly zero (Table 2). The corresponding analysis for **P–26N–P** and **P–27N–P** reveals an identical story. These differences exhibit a quantum effect that is intimately related to the mechanism of SF. Triplet pair formation will be fast in compounds that satisfy the twin requirements of a strong CT_{CC} contribution to the wavefunction and a strong dipole coupling to the ground state, a feature that appears directly in the optical absorption spectra.

Importantly, the predicted strength of the CT absorption between the DQI and CQI compounds with Ph and N linkers agrees

https://doi.org/10.1038/s41557-022-01107-8

Table 2 | Characteristics of CT states for PβP and TβT

SFC	β	E (eV)	μ	CT_{cc}	$CT_{cβ}$	$LE_β$
Tetracene	**26N**	3.45	1.67	0.47	0.17	0.12
	27N	3.55	0.06	0.57	0.14	0.08
	26A	3.54	1.61	0.33	0.28	0.41
		3.78	0.87	0.52	0.19	0.15
	27A	3.57	0.50	0.39	0.29	0.33
		3.77	0.40	0.45	0.20	0.16
Pentacene	**26N**	3.11	0.99	0.55	0.10	0.05
		3.33	0.68	0.22	0.08	0.05
	27N	3.18	0.03	0.60	0.08	0.03
		3.31	0.74	0	0.09	0.03
	26A	3.05	1.46	0.26	0.25	0.48
		3.24	0.50	0.51	0.04	0.47
		3.34	0.44	0.16	0.05	0.31
		3.54	1.65	0.16	0.30	0.39
	27A	3.11	0.37	0.24	0.25	0.55
		3.25	0.31	0.53	0.05	0.38
		3.34	0.46	0.02	0.08	0.39
		3.57	0.46	0.18	0.32	0.33

Calculated energies, transition dipole couplings with the ground state and wavefunction characteristics. μ is the transition dipole coupling with ground state (Å, electronic charge e=1).

with experimental absorption spectra and strongly correlates to the relative magnitude of τ_{SF}. In the CQI compounds (β = **14Ph** and **26N**), we observed a single additional peak (absent in the monomer spectra) centred at 3 eV for TβT (Fig. 4c and Supplementary Fig. 9) and 2.64 eV for PβP (Supplementary Fig. 8). In the corresponding DQI compounds (β = **13Ph** and **27N**), this peak is largely absent. The CT states in CQI **T**–**26N**–**T** and **P**–**26N**–**P** were optically allowed and had a substantial contribution from configurations with CT between the terminal chromophores (Table 2) and feature fast SFs: τ_{SF} = 30 and 56 ps, respectively. The corresponding states in DQI **T**–**27N**–**T** and **P**–**27N**–**P** either had weak dipole coupling to the ground state or weak contributions from configurations with a direct CT (τ_{SF} = 952 and 882 ps, respectively). A detailed analysis of the correlated electron exciton-basis wavefunctions of the excited states for all the compounds shows that this is a general requirement (Table 2).

The rules that govern QI with A as the bridge molecule are more complex due to two competing quantum effects, which modify the nature and energetics of the virtual CT states involved in SF and lead to a relatively small τ_{SF} in the DQI compounds. First, the absence of a long-range antiferromagnetic order in one dimension[43] implies that, for long bridge molecules, spin couplings between distant atoms are not strictly antiferromagnetic or ferromagnetic. As a result, CTs between carbon atoms at the points of connectivity become optically allowed, which includes DQI compounds, and the graphical model of Fig. 1 becomes less rigorous. Second, in A-bridged SFCs, the excited-state wavefunctions of the optically allowed CT transitions contain considerable bridge-resonance contributions (Table 2). For example, in **T**–**26A**–**T** and **T**–**27A**–**T**, the relative weights of the three dominant constituents of the eigenstates at ~3.55 and ~3.75 eV involve $CT_{cβ}$, CT_{cc} and LE_A with roughly equivalent amplitudes. Unlike the naphthalene case, the transition dipole couplings to these states in DQI **T**–**27A**–**T** are non-zero and only ~2–3 times smaller than the equivalent transition in the CQI **T**–**26A**–**T**. A qualitatively similar picture was observed in the eigenstates of **P**–**26A**–**P** and **P**–**27A**–**P**, with a slightly larger difference in the transition dipole couplings between CQI and DQI (~3–4 times smaller). These results explain our observation of only about a 4–5 times change in τ_{SF} between CQI **26A** connectivity and DQI **27A** connectivity. Furthermore, although the SF in DQI **P**–**27A**–**P** is relatively slow, it is still notably faster than those in **T**–**27N**–**T** and **P**–**27N**–**P**.

In support of the above model, we observed several peaks in the CT region of the experimental absorption spectra for both DQI **27A** and CQI **26A** bridge compounds. The relative intensities of this series of peaks varied with connectivity. For example, in the **T**–**27A**–**T** DQI compound, the dominant transition was centred near 2.95 eV, with weak shoulders offset by approximately 0.2 eV on either side of the main transition. In the CQI analogue (**T**–**26A**–**T**), the main peak was reduced in intensity but the relative oscillator strength of the shoulders increased. A more pronounced effect was observed in PβP, where the relative intensity of the shoulders became larger than that of the primary peak in **P**–**26A**–**P** (Supplementary Fig. 8). Although previous theoretical treatments of the absorption spectra in directly bonded acene oligomers suggested that bright CT-type transitions can emerge in cases of strong chromophore–chromophore coupling[44], neither the effect of the chemical bridge nor implications for the SF dynamics were considered. Here we see that both a large CT_{cc} contribution to the CT excitation and a strong transition dipole moment are essential for a fast iSF. The former is a signature of direct quantum mechanical coupling between the SFCs, whereas the latter ensures that virtual excitation of the CT excited state efficiently couples the singlet and triplet pair states (Supplementary Information)[25,40]. We note that although the role of virtual CT states in mediating the rate of SF has long been inferred, these data represent fundamental evidence of such an effect[45–49].

Conclusion

This work poses a paradigm shift to understand the mechanism of iSF in which DCI and CQI play an essential role. Graphical models to predict QI based on connectivity are successful in single-molecule electronics, but these models are not as obviously applied to light-induced processes that involve exciton transport in DBA systems. Here, QI graphical models can be implemented to describe multiexciton formation as a function of connectivity in a variety of acene bridges, which is effective, in part, due to the spatially symmetric nature of the intramolecular SFCs. The QI effects were also predicted by the model in discretely asymmetric chromophores, which do not have a marked asymmetry, as in the case of conventional electron-rich and poor DBAs. We note that QI involves the electronic wavefunctions, and as such determine the SF rate constants. Decorrelation of a [TT] state and subsequent recombination processes depend, instead, on the spin Hamiltonian with anisotropic interactions, which is strongly influenced by the proximity of triplet excitons. These systems will further allow us to establish the connection between the 'ferromagnetic' or 'antiferromagnetic' coupling imparted by the connectivity and QI effects[25,39]. We also found that both bridge resonance contributions and structural distortion that arise from steric interactions with the chromophores also impact triplet pair formation and the magnitude of the QI effects. Briefly, for short π-bridge lengths, CT interactions between the SFCs mediate SF and the models that govern QI resemble those from single-molecule transport. However, for longer π bridges, additional contributions to the excited-state wavefunctions from optically allowed CT and local excitations that involve the bridge further accelerate triplet pair formation. Although QI remains impactful in these systems, the differences are smaller between DQI and CQI connectivity. The general implications of this work reflect the need to investigate the extent to which graphical models translate into various classes of bridges, for example, non-alternant hydrocarbons[50,51] and those that impart cross-conjugation[7] (cyclic and acyclic), among other types. It is also important to highlight that the remarkable correlation between QI and diradicaloid character in single-molecule transport[51], which led to a predictive power in key design features of single-molecule devices, can also be extended to iSF. Therefore, the understanding of the link

between electronic-structure contributions and QI to the fundamental principles of triplet pair evolution is important to optimize the formation of entangled spin states and thus amplify opportunities to be implemented in quantum information technologies.

Online content

Any methods, additional references, Nature Portfolio reporting summaries, source data, extended data, supplementary information, acknowledgements, peer review information; details of author contributions and competing interests; and statements of data and code availability are available at https://doi.org/10.1038/s41557-022-01107-8.

References

1. Su, T. A., Neupane, M., Steigerwald, M. L., Venkataraman, L. & Nuckolls, C. Chemical principles of single-molecule electronics. *Nat. Rev. Mater.* **1**, 16002 (2016).
2. Lambert, C. J. Basic concepts of quantum interference and electron transport in single-molecule electronics. *Chem. Soc. Rev.* **44**, 875–888 (2015).
3. Jan van der Molen, S. & Liljeroth, P. Charge transport through molecular switches. *J. Phys. Condens. Matter* **22**, 133001 (2010).
4. Guédon, C. M. et al. Observation of quantum interference in molecular charge transport. *Nat. Nanotechnol.* **7**, 305–309 (2012).
5. Arroyo, C. R. et al. Signatures of quantum interference effects on charge transport through a single benzene ring. *Angew. Chem. Int. Ed.* **52**, 3152–3155 (2013).
6. Solomon, G. C. et al. Understanding quantum interference in coherent molecular conduction. *J. Chem. Phys.* **129**, 054701 (2008).
7. Tsuji, Y., Hoffmann, R., Strange, M. & Solomon, G. C. Close relation between quantum interference in molecular conductance and diradical existence. *Proc. Natl Acad. Sci. USA* **113**, E413–E419 (2016).
8. Markussen, T., Stadler, R. & Thygesen, K. S. The relation between structure and quantum interference in single molecule junctions. *Nano Lett.* **10**, 4260–4265 (2010).
9. Ortiz, R. et al. Exchange rules for diradical π-conjugated hydrocarbons. *Nano Lett.* **19**, 5991–5997 (2019).
10. Gorczak, N. et al. Computational design of donor–bridge–acceptor systems exhibiting pronounced quantum interference effects. *Phys. Chem. Chem. Phys.* **18**, 6773–6779 (2016).
11. Gorczak, N. et al. Charge transfer versus molecular conductance: molecular orbital symmetry turns quantum interference rules upside down. *Chem. Sci.* **6**, 4196–4206 (2015).
12. Sanders, S. N. et al. Exciton correlations in intramolecular singlet fission. *J. Am. Chem. Soc.* **138**, 7289–7297 (2016).
13. Pun, A. B. et al. Ultra-fast intramolecular singlet fission to persistent multiexcitons by molecular design. *Nat. Chem.* **11**, 821–828 (2019).
14. Krishnapriya, K. C. et al. Spin density encodes intramolecular singlet exciton fission in pentacene dimers. *Nat. Commun.* **10**, 33 (2019).
15. Hetzer, C., Guldi, D. M. & Tykwinski, R. R. Pentacene dimers as a critical tool for the investigation of intramolecular singlet fission. *Chem. Eur. J.* **24**, 8245–8257 (2018).
16. Basel, B. S. et al. Influence of the heavy-atom effect on singlet fission: a study of platinum-bridged pentacene dimers. *Chem. Sci.* **10**, 11130–11140 (2019).
17. Margulies, E. A. et al. Enabling singlet fission by controlling intramolecular charge transfer in π-stacked covalent terrylenediimide dimers. *Nat. Chem.* **8**, 1120–1125 (2016).
18. Sakuma, T. et al. Long-lived triplet excited states of bent-shaped pentacene dimers by intramolecular singlet fission. *J. Phys. Chem. A* **120**, 1867–1875 (2016).
19. Nakamura, S. et al. Enthalpy–entropy compensation effect for triplet pair dissociation of intramolecular singlet fission in phenylene spacer-bridged hexacene dimers. *J. Phys. Chem. Lett.* **12**, 6457–6463 (2021).
20. Korovina, N. V. et al. Linker-dependent singlet fission in tetracene dimers. *J. Am. Chem. Soc.* **140**, 10179–10190 (2018).
21. Ito, S., Nagami, T. & Nakano, M. Design principles of electronic couplings for intramolecular singlet fission in covalently-linked systems. *J. Phys. Chem. A* **120**, 6236–6241 (2016).
22. Paul, S., Govind, C. & Karunakaran, V. Planarity and length of the bridge control rate and efficiency of intramolecular singlet fission in pentacene dimers. *J. Phys. Chem. B* **125**, 231–239 (2021).
23. Abraham, V. & Mayhall, N. J. Revealing the contest between triplet–triplet exchange and triplet–triplet energy transfer coupling in correlated triplet pair states in singlet fission. *J. Phys. Chem. Lett.* **12**, 10505–10514 (2021).
24. Abraham, V. & Mayhall, N. J. Simple rule to predict boundedness of multiexciton states in covalently linked singlet-fission dimers. *J. Phys. Chem. Lett.* **8**, 5472–5478 (2017).
25. Chesler, R., Khan, S. & Mazumdar, S. Wave function based analysis of dynamics versus yield of free triplets in intramolecular singlet fission. *J. Phys. Chem. A* **124**, 10091–10099 (2020).
26. Herrmann, C. Electronic communication as a transferable property of molecular bridges? *J. Phys. Chem. A* **123**, 10205–10223 (2019).
27. Walter, D., Neuhauser, D. & Baer, R. Quantum interference in polycyclic hydrocarbon molecular wires. *Chem. Phys.* **299**, 139–145 (2004).
28. Bajaj, A., Kaur, P., Sud, A., Berritta, M. & Ali, Md. E. Anomalous effect of quantum interference in organic spin filters. *J. Phys. Chem. C* **124**, 24361–24371 (2020).
29. Sanders, S. N. et al. Quantitative intramolecular singlet fission in bipentacenes. *J. Am. Chem. Soc.* **137**, 8965–8972 (2015).
30. Parenti, K. R. et al. Bridge resonance effects in singlet fission. *J. Phys. Chem. A* **124**, 9392–9399 (2020).
31. Zirzlmeier, J. et al. Singlet fission in pentacene dimers. *Proc. Natl Acad. Sci. USA* **112**, 5325–5330 (2015).
32. Korovina, N. V., Pompetti, N. F. & Johnson, J. C. Lessons from intramolecular singlet fission with covalently bound chromophores. *J. Chem. Phys.* **152**, 040904 (2020).
33. Davis, W. B., Svec, W. A., Ratner, M. A. & Wasielewski, M. R. Molecular-wire behaviour in *p* -phenylenevinylene oligomers. *Nature* **396**, 60–63 (1998).
34. Fuemmeler, E. G. et al. A direct mechanism of ultrafast intramolecular singlet fission in pentacene dimers. *ACS Cent. Sci.* **2**, 316–324 (2016).
35. Yablon, L. M. et al. Singlet fission and triplet pair recombination in bipentacenes with a twist. *Mater. Horiz.* **9**, 462–470 (2022).
36. Quinn, J. R., Foss, F. W., Venkataraman, L., Hybertsen, M. S. & Breslow, R. Single-molecule junction conductance through diaminoacenes. *J. Am. Chem. Soc.* **129**, 6714–6715 (2007).
37. Pariser, R. & Parr, R. G. A semi-empirical theory of the electronic spectra and electronic structure of complex unsaturated molecules. I. *J. Chem. Phys.* **21**, 466–471 (1953).
38. Pople, J. A. Electron interaction in unsaturated hydrocarbons. *Trans. Faraday Soc.* **49**, 1375 (1953).
39. Smith, M. B. & Michl, J. Recent advances in singlet fission. *Annu. Rev. Phys. Chem.* **64**, 361–386 (2013).
40. Berkelbach, T. C., Hybertsen, M. S. & Reichman, D. R. Microscopic theory of singlet exciton fission. II. Application to pentacene dimers and the role of superexchange. *J. Chem. Phys.* **138**, 114103 (2013).
41. Khan, S. & Mazumdar, S. Diagrammatic exciton basis theory of the photophysics of pentacene dimers. *J. Phys. Chem. Lett.* **8**, 4468–4478 (2017).

42. Khan, S. & Mazumdar, S. Theory of transient excited state absorptions in pentacene and derivatives: triplet–triplet biexciton versus free triplets. *J. Phys. Chem. Lett.* **8**, 5943–5948 (2017).
43. Kittel, C. & Fong, C. Y. *Quantum Theory of Solids* (Wiley, 1987).
44. Hele, T. J. H. et al. Anticipating acene-based chromophore spectra with molecular orbital arguments. *J. Phys. Chem. A* **123**, 2527–2536 (2019).
45. Beljonne, D., Yamagata, H., Brédas, J. L., Spano, F. C. & Olivier, Y. Charge-transfer excitations steer the Davydov splitting and mediate singlet exciton fission in pentacene. *Phys. Rev. Lett.* **110**, 226402 (2013).
46. Basel, B. S. et al. Evidence for charge-transfer mediation in the primary events of singlet fission in a weakly coupled pentacene dimer. *Chem* **4**, 1092–1111 (2018).
47. Busby, E. et al. A design strategy for intramolecular singlet fission mediated by charge-transfer states in donor–acceptor organic materials. *Nat. Mater.* **14**, 426–433 (2015).
48. He, G. et al. Charge transfer states impact the triplet pair dynamics of singlet fission polymers. *J. Chem. Phys.* **153**, 244902 (2020).
49. Monahan, N. & Zhu, X.-Y. Charge transfer-mediated singlet fission. *Annu. Rev. Phys. Chem.* **66**, 601–618 (2015).
50. Tsuji, Y. & Yoshizawa, K. Frontier orbital perspective for quantum interference in alternant and nonalternant hydrocarbons. *J. Phys. Chem. C* **121**, 9621–9626 (2017).
51. Xia, J. et al. Breakdown of interference rules in azulene, a nonalternant hydrocarbon. *Nano Lett.* **14**, 2941–2945 (2014).

Methods

Synthesis

The synthesis of pentacene- and tetracene-bridged dimers with β = **14Ph**, **26N** and **26A** was reported previously[29,30]. Similar cross-coupling conditions were used to synthesize β = **13Ph**, **27N**, **15N**, **16N** and **27A**, as detailed in the Supplementary Information. We note that TIPS (triisopropylsilylethynyl) groups are installed on all the anthracene, tetracene and pentacene chromophores for solubility and stability.

Ultrafast spectroscopy

The iSF dynamics of the series were characterized by transient absorption spectroscopy. The protocol for identifying iSF in solution is well-established[13,29,52] (additional details provided in the Supplementary Information). Briefly, a dilute solution of a compound in solution (~50 μM in toluene) was pumped by a laser pulse resonant with a vibrational excited state of the S_1 exciton. The broadband transient response was measured across the ground state bleach ($S_0 \rightarrow S_1$ transition) as well as the singlet ($S_1 \rightarrow S_n$ transition) and triplet ($T_1 \rightarrow T_n$ transition) PIA features. The singlet exciton on pentacene is identified by a characteristic broad PIA between 400 and 575 nm that decays commensurate with the rise of the triplet exciton, characterized by its narrow PIA feature that peaked at around 520 nm. A similar set of extensively characterized PIA features can be used to quantify the singlet-to-triplet formation rate in tetracene-based compounds. The assignment of triplet excitons in these compounds was verified through triplet sensitization measurements based on collisional energy transfer. Comparison of the photoexcited and sensitized triplet properties allowed us to distinguish individual triplets (formed by intersystem crossing, for example) from triplet pairs formed by SF. In general, the SF-generated triplet pair and individual sensitized triplet show similar transient spectra but differ markedly in their recombination dynamics, as triplet pairs exhibit a characteristic triplet–triplet annihilation process that leads to a biexponential decay of the overall triplet population. Standard global analysis procedures were used to obtain deconvoluted spectra and extract time constants. For all the compounds used in this study, the overall SF yield was determined from kinetic arguments that compared the relative rates of singlet decay to the ground state ($S_1 \rightarrow S_0$) to decay via triplet pair formation ($S_1 \rightarrow {}^1(TT)$). Further discussion of the yields can be found in the Supplementary Information. Importantly, no other photoproducts were observed in this series of compounds, which permits a direct comparison of the rate constants.

Quantum chemical calculations

The π-electron only PPP Hamiltonian is written as[37,38]:

$$H = \sum_{ij,\sigma} t_{ij}\left(C^{\dagger}_{i\sigma}C_{j\sigma} + C^{\dagger}_{j\sigma}C_{i\sigma}\right) + U\sum_{i} n_{i\uparrow}n_{i\downarrow} + \sum_{i<j} V_{ij}\left(n_i - 1\right)\left(n_j - 1\right)$$

Here, $C^{\dagger}_{i\sigma}$ creates an electron with spin σ on the p_z orbital of carbon (C) atom i, $n_{i\sigma} = \sum_i C^{\dagger}_{i\sigma}C_{i\sigma}$ is the number of electrons with spin σ on atom i and $n_i = \sum_\sigma n_{i\sigma}$ is the total number of electrons on the atom. We retained electronic hoppings t_{ij} only between the nearest neighbours i and j. U is the Coulomb repulsion between two electrons that occupy the p_z orbital of the same C atom, and V_{ij} is the long-range Coulomb interaction. The average bond lengths within an acene unit are different for the peripheral (1.40 Å) and internal (1.46 Å) bonds. Based on widely used bond-length-hopping integral relationships[53], we chose intra-acene peripheral (internal) hopping integrals t_{ij} as 2.4 (2.2) eV. We chose planar geometries for both and therefore interunit hopping integrals of 2.2 eV between the SFC monomers and the bridge molecules, although this can be relaxed[54]. We use the screened Ohno parameterization for the long-range Coulomb repulsion, $V_{ij} = U/\kappa(1 + 0.6117R^2_{ij})^{1/2}$, where R_{ij} is the distance in Å between C atoms i and j, and κ is an effective dielectric constant[41,42,55]. Based on our previous work[56], we chose U = 7.7 eV and κ = 1.3.

Our calculations use the molecular exciton basis, with Hartree–Fock MOs localized on individual monomers[41,55,56]. Depending on the compound, we retained between 24 to 30 exciton-basis MOs, of which 4–6 were localized on the bridge molecules, with equal numbers of bonding and antibonding MOs (see Supplementary Information). Further details may be found in previous studies[24,25,41,42,55,56] and in the Supplementary Information. To arrive at the precise description of the two electron–two hole $^1(TT)$ excitation, we used the multiple reference singles and doubles configuration interaction approach[42,53,57], which includes configuration interactions with the most dominant four electron–four hole excitations. The total number of many-electron configurations retained to describe any single eigenstate was several million. In addition to the wavefunctions and energies, we also calculated the transition dipole couplings from the ground state to all the excited states and the linear absorption spectra.

Data availability

The raw transient absorption data used to generate Figs. 2 and 3 and the corresponding analysis are freely available via the Dryad public repository: https://doi.org/10.5061/dryad.x95x69pnn. Additional data are available upon request. Source data are provided with this paper.

References

52. Kumarasamy, E. et al. Tuning singlet fission in π-bridge-π chromophores. *J. Am. Chem. Soc.* **139**, 12488–12494 (2017).
53. Aryanpour, K., Shukla, A. & Mazumdar, S. Theory of singlet fission in polyenes, acene crystals, and covalently linked acene dimers. *J. Phys. Chem. C* **119**, 6966–6979 (2015).
54. Ramasesha, S., Albert, I. D. L. & Sinha, B. Optical and magnetic properties of the exact PPP states of biphenyl. *Mol. Phys.* **72**, 537–547 (1991).
55. Khan, S. & Mazumdar, S. Optical probes of the quantum-entangled triple–triplet state in a heteroacene dimer. *Phys. Rev. B* **98**, 165202 (2018).
56. Chandross, M. & Mazumdar, S. Coulomb interactions and linear, nonlinear, and triplet absorption in poly(*para*-phenylenevinylene). *Phys. Rev. B* **55**, 1497–1504 (1997).
57. Tavan, P. & Schulten, K. Electronic excitations in finite and infinite polyenes. *Phys. Rev. B* **36**, 4337–4358 (1987).

Acknowledgements

This work was supported by the US Department of Energy, Office of Science, Office of Basic Energy Sciences under award no. DE-SC0022036 (M.Y.S. and L.M.C.) and the National Science Foundation under award no. CHE-1764152 (S.M.). K.R.P. thanks the Department of Defense for a National Defense Science and Engineering (NDSEG) Fellowship. J.Z. thanks the Columbia College Science Scholars Program and Guthikonda Fellowship. X.Y. acknowledges the Beijing Institute of Technology Research Fund Program for Young Scholars, and the Analysis and Testing Center of Beijing Institute of Technology for NMR and mass spectrometry characterization. This research used resources at the Center for Functional Nanomaterials, which is a US DOE Office of Science Facility at Brookhaven National Laboratory under contract DE-SC0012704.

Author contributions

S.M., M.Y.S and L.M.C. oversaw the project. K.R.P., M.Y.S. and L.M.C. designed the molecules. G.H. collected the transient absorption spectroscopy data and K.R.P., G.H. and M.Y.S. carried out data analysis.

K.R.P., B.X., H.H., D.M. and J.Z. synthesized and characterized the molecules, supervised by X.Y. and L.M.C. The theory models were designed by S.M. and A.S. PPP calculations were carried out by R.C. and P.B. Density functional theory calculations were carried out by G.H. The paper was written by K.R.P., S.M., M.Y.S. and L.M.C. with contributions from all authors.

Competing interests
The authors declare no competing financial interests.

Additional information
Extended data is available for this paper at https://doi.org/10.1038/s41557-022-01107-8.

Supplementary information The online version contains supplementary material available at https://doi.org/10.1038/s41557-022-01107-8.

Correspondence and requests for materials should be addressed to Sumit Mazumdar, Matthew Y. Sfeir or Luis M. Campos.

Peer review information *Nature Chemistry* thanks Ferdinand Grozema and the other, anonymous, reviewer(s) for their contribution to the peer review of this work.

https://doi.org/10.1038/s41557-022-01107-8

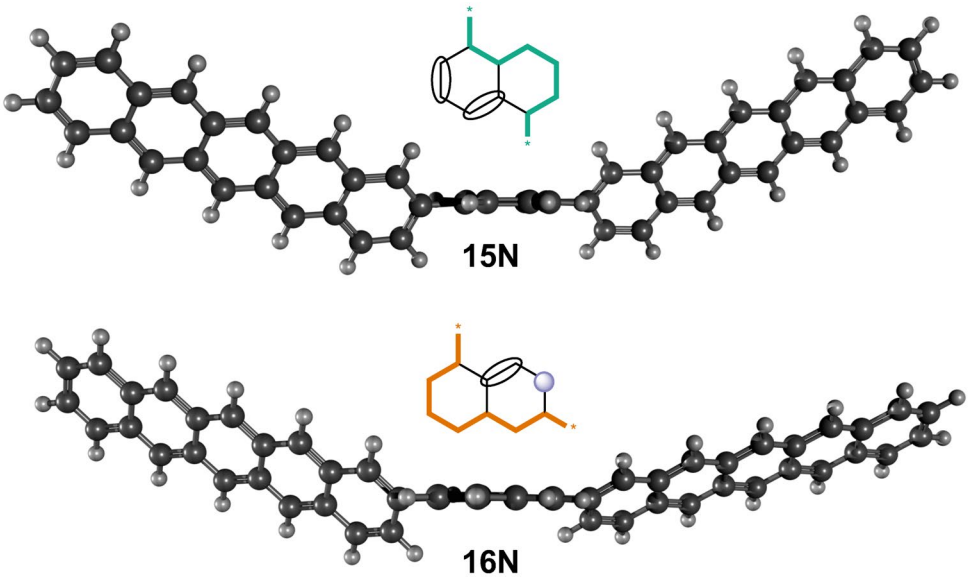

Extended Data Fig. 1 | Density functional theory geometry calculations. The ground state geometry of **P**–**15N**–**P** and **P**–**16N**–**P** are optimized using density functional theory (DFT) at the B3LYP/6-31G(d) level. Substitution at the 2, 6 and 7 positions of naphthalene gives a dihedral angle of ~35°, consistent with previous calculations on acene dimers[10]. Substitution at the 1 and 5 positions of naphthalene gives a more distorted structure with a dihedral angle of ~58°. As has been previously shown, singlet fission slows down considerably in highly twisted dimers[10,11]. We show the geometry of the twisted dimers and summarize all the naphthalene substitution positions and calculated dihedral angles in Extended Data Fig. 2.

https://doi.org/10.1038/s41557-022-01107-8

β	dihedral angle
15N	58° (1), 58° (5)
16N	58° (1), 35° (6)
26N	35° (2), 35° (6)
27N	35° (2), 35° (7)

Extended Data Fig. 2 | Naphthalene substitution and corresponding dihedral angles calculated with DFT.

https://doi.org/10.1038/s41557-022-01107-8

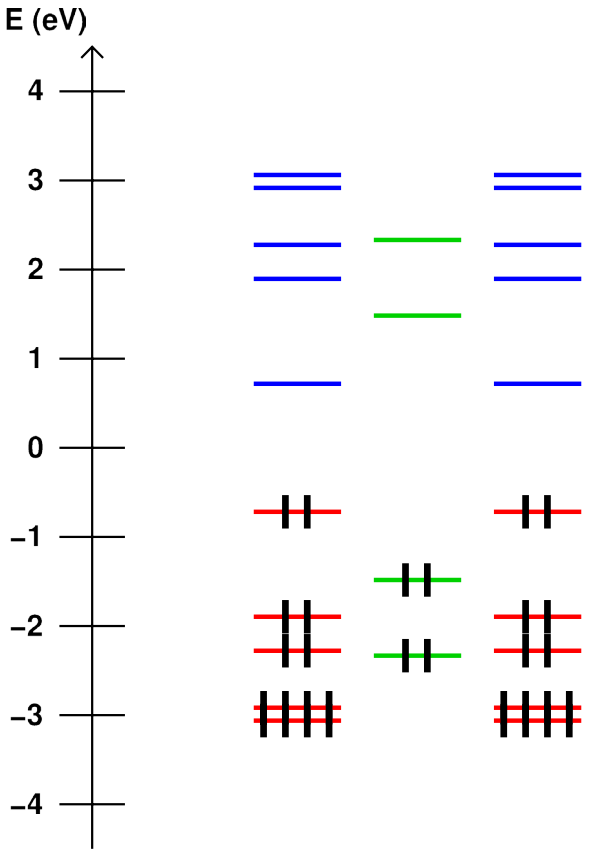

Extended Data Fig. 3 | Hückel energy level distribution for T–N–T displaying the active space of 24 MOs. The MRSDCI calculations are over an active space of MOs about the chemical potential that is smaller than the complete set. The lowest few bonding MOs are frozen (that is, excitations from these lowest MOs are not included in the CI calculations) and the highest MOs related to these by charge-conjugation symmetry are excluded from the active space. As of now, we have performed MRSDCI calculations over active spaces of 22–30 MOs, 11–15 bonding and 11–15 antibonding. These are absolutely the largest active spaces over which calculations of $^1|TT\rangle$ have ever been done. We illustrate our procedure with the specific case of T–N–T. The localized tetracene Hückel bonding (red) and antibonding (blue) MOs, and the naphthalene (green) MOs constitute the active MO space in our T–N–T calculations. For calculations on T–Ph–T, T–A–T, P–Ph–P, P–N–P and P–A–P, we retained 20 + 4, 16 + 6, 20 + 4, 20 + 6 and 20 + 6 MOs, respectively, where the numbers in each sum indicate the chromophore MOs plus the linker MOs.

https://doi.org/10.1038/s41557-022-01107-8

Compounds	τ_{SF} (ps)	$\tau_{(TT)}$ (ns)	τ_{T1} (μs)
P–14Ph–P	17	16	25
P–13Ph–P	391	189	24
P–26N–P	56	55	15
P–27N–P	882	277	30
P–15N–P	1053	220	28
P–16N–P	1815	91	23
P–26A–P	48	103	21
P–27A–P	253	270	20
T–14Ph–T	7	121	141
T–13Ph–T	453	129	145
T–26N–T	30	140	136
T–27N–T	952	129	160
T–15N–T	591	141	170
T–16N–T	1437	23	158
T–26A–T	14	157	133
T–27A–T	55	126	155

Extended Data Fig. 4 | Time constants for singlet fission, triplet pair decay and free triplet decay. Uncertainties are +/− 5%.